Direct switching of polarization vortex in triangular ferroelectric nanodots: Role of crystal orientation

Le Van Lich [ORCID],[1,*] Minh-Tien Le [ORCID],[1] Ngoc-Lu Vu,[1] Hong-Dang Nguyen [ORCID],[1] Van-Tuan Le [ORCID],[2] Minh-Tan Ha,[3] Trong-Giang Nguyen,[1] and Van-Hai Dinh[1]

[1]*School of Materials Science and Engineering, Hanoi University of Science and Technology, No. 1, Dai Co Viet Street, Hanoi 100000, Vietnam*
[2]*School of Mechanical Engineering, Hanoi University of Science and Technology, No. 1, Dai Co Viet Street, Hanoi 100000, Vietnam*
[3]*Energy and Environmental Division, Korea Institute of Ceramic Engineering and Technology, Jinju-si 52851, Korea*

Attaining an energy-efficient pathway to switch the rotation of polarization vortex with the use of trivial homogeneous electric field is essentially important for low-power consumption electronic nanodevices, yet still challenging. In this study, we systematically investigate the switching behaviors of polarization vortex in triangular ferroelectric nanodots with different crystal orientations. The obtained results exhibit diversity pathways for the vortex switching, including both indirect and direct switching, which depend on the crystal orientation. In the indirect pathway, the switching process requires a destruction of initial vortex domain structure to form a rectilinear domain at a large electric field. Otherwise, in the direct switching pathway, the initial vortex is switched to an opposite one without the stabilization of an intermediate state. Importantly, the direct pathway requires a lower switching field compared to that in the indirect ones. We further elucidate the temporal evolution of domain structure during the direct switching of polarization vortex in the triangular nanodot. A comprehensive viewpoint on the effect of crystal orientation is expressed, from which the advantages of direct switching are clarified. The present study suggests an efficient route on the practical control of vortex rotation in ferroelectric nanostructures under homogeneous electric field.

I. INTRODUCTION

Numerous scientific breakthroughs have been achieved in the past decade with the discoveries of new exotic polar topological states, including vortex [1], skyrmion [2], hedgehog [3], and meron [4] states. These findings lead to plenty of emerging physical phenomena and open a broad avenue toward future topological electronic nanodevices [5–7]. Particularly, the recent advance in structural characterization, which achieves a high spatial resolution down to atomic scale, has enabled the realization of polarization vortex patterns in ferroelectric nanostructures [8–10]. The emergence of equilibrium polarization vortex can significantly reduce the depolarization field, which is induced by the interruption of polarization at free surfaces or interfaces of ferroelectric nanostructures [1,8]. In the vortex structure, the polarization field continuously rotates through the space; but such continuous rotation is disrupted at a singular point, i.e., the vortex core, which constitutes a topological defect [11]. The existence of topological defects, such as the vortex core, accumulates a high energy density in the vicinity of the core due to the large gradients of polarization and strain fields [12], and therefore, gives rise to exotic properties, such as superfine conductive channels [13,14], nonlinear optical properties [15], giant enhancement of local nanoscale piezoelectric

response [16], and unique negative capacitance [17,18]. The polarization vortex is characterized by its vorticity (or toroidal moment) [19] and geometrically distinguishable by its clockwise (CW) or counterclockwise (CCW) rotations. Importantly, exploring a practical and energy-efficient pathway, which can switch the vortex rotation from one to another state through external stimuli, is highly desired from both academic importance and technological applications.

Since the polarization vortex is formed at a delicate balance among several energy contributions, such as electrostatic, electromechanical, gradient, and elastic energies, an application of external stimuli may disrupt this energetic balance. Consequently, the transition of polarization vortex is possible, in spite of its topological protection against low fields [11]. Theoretically, several strategies have been proposed for the vortex switching based on the rational control of extrinsic factors, such as electric and mechanical fields [12,20–22], geometrical nanostructures [23,24], defects [25,26], and composition distributions [27]. For instance, early ideas have used curled or inhomogeneous electric fields to switch the vortex rotation because of the conjugation between these fields and the toroidal moment of polarization vortex [20,21]. Mechanical approaches are feasible to control the vortex rotation [12,22]. Designed geometries of ferroelectric nanostructures have also been demonstrated to enable switching of polarization vortex through geometry-induced symmetry breaking of the vortex structure [23]. In addition, material design, which can break spatial inversion symmetry at a scale beyond the

*lich.levan@hust.edu.vn

024104-1

unit-cell level and enables to stabilize an asymmetric vortex, has also been proven for the control of vortex rotation [27]. Experimentally, numerous efforts have been devoted to observing the topological transformation of polarization structures. Recent progresses in experiments have made a great step toward the electrical and mechanical manipulations of polarization vortex in ferroelectric superlattices and successfully observed topological transformations of polar structures with the spatial resolution down to atomic scale [28–31].

The mentioned strategies have demonstrated various possibilities for the switching of polarization vortex, however, the switching pathways commonly destruct the single vortex to generate a rectilinear domain or multiple vortex structures, before a single vortex with reverse rotation is formed. These intermediate domain structures are topologically distinguishable from the single vortex [32]. Energetically, this switching pathway is inefficient since a large electric or mechanical field is commonly required to clear away the single-vortex structure. In addition, such an indirect pathway has a long switching duration since it involves several successive processes of phase transitions. Until quite recently, very few attempts have been made to find an approach that can directly switch the vortex rotation. For example, polarization vortex can be directly switched back and forth between CCW and CW rotations by a sweeping biased tip over a homogeneous ferroelectric nanodot [33] or applying an homogeneous electric field to a compositionally graded ferroelectric nanodot [27]. Therefore, more effective approaches should be proposed, which can directly switch the polarization vortex. However, previous studies have shown that the incompatibility between geometries of nanostructures and crystal orientation of ferroelectrics can greatly disturb the polarization field, which brings about unusual switching behavior of domain structures [34,35]. Therefore, it is expected that the switching behavior of polarization vortex can be tailored with the control of crystal orientation in ferroelectric nanostructures. However, the effect of ferroelectric crystal orientation in incompatible nanostructures on the vortex switching has not been explored.

In this work, a phase field model of ferroelectrics that accounts for the effect of crystal orientation is constructed to study the switching behavior of polarization vortex in a low-symmetric nanodot with triangular geometry. The crystal orientation is assumed to rotate in plane of the triangular nanodot. Several switching pathways of polarization vortex under homogeneous electric field are obtained and presented in a dependence with the crystal orientation. Both direct and indirect switching pathways of the polarization vortex can be realized. In addition, the energy-efficient switching pathway is suggested and discussed.

II. METHODOLOGY

A. Constitutive relations

A three-dimensional phase field model is constructed on the basis of Ginzburg-Landau theory to investigate the polarization switching under the electric field in triangular nanodots with different crystal orientations [36,37]. The total free energy F of the ferroelectric system can be expressed as

$$
\begin{aligned}
F(\boldsymbol{p}, \boldsymbol{\varepsilon}, \boldsymbol{\phi}) &= \int_V f(\boldsymbol{p}, \nabla\boldsymbol{p}, \boldsymbol{\varepsilon}, \boldsymbol{\phi}) dV \\
&= \int_V [f_{\mathrm{Pol}}(\boldsymbol{p}) + f_{\mathrm{Grad}}(\nabla\boldsymbol{p}) \\
&\quad + f_{\mathrm{Elas}}(\boldsymbol{\varepsilon}, \boldsymbol{p}) + f_{\mathrm{Elec}}(\boldsymbol{p}, \boldsymbol{\phi})] dV,
\end{aligned} \tag{1}
$$

where, V is the volume of ferroelectric material; $\boldsymbol{p}, \nabla\boldsymbol{p}, \boldsymbol{\varepsilon}$, and $\boldsymbol{\phi}$ refer to polarization, gradient of polarization, strain, and electric potential, respectively. In Eq. (1), $f_{\mathrm{Pol}}(\boldsymbol{p})$, $f_{\mathrm{Grad}}(\nabla\boldsymbol{p})$, $f_{\mathrm{Elas}}(\boldsymbol{\varepsilon}, \boldsymbol{p})$, and $f_{\mathrm{Elec}}(\boldsymbol{p}, \boldsymbol{\phi})$ denote the densities of polarization (or Landau), gradient, mechanical, and electrostatic energies, respectively. The polarization energy density can be described as

$$
\begin{aligned}
f_{\mathrm{Pol}}(\boldsymbol{p}) &= \alpha_i \left(p_i^L\right)^2 + \alpha_{ij}\left(p_i^L\right)^2\left(p_j^L\right)^2 \\
&\quad + \alpha_{ijk}\left(p_i^L\right)^2\left(p_j^L\right)^2\left(p_k^L\right)^2,
\end{aligned} \tag{2}
$$

where α_i, α_{ij}, and α_{ijk} ($i, j, k = 1, 2, 3$) are thermodynamic coefficients; p_i^L are polarization components in the local crystallographic coordinate system. In the global Cartesian coordinates (x_1, x_2, x_3), the crystal orientation is described by using three Euler angles (α, β, θ) with respect to the global axes. The transformation matrix R from the global to local coordinate systems is given as

$$
R = \begin{pmatrix} \cos\alpha \cos\theta - \sin\alpha \cos\beta \sin\theta & \sin\alpha \cos\theta + \cos\alpha \cos\beta \sin\theta & \sin\beta \sin\theta \\ -\cos\alpha \sin\theta - \sin\alpha \cos\beta \cos\theta & -\sin\alpha \sin\theta + \cos\alpha \cos\beta \cos\theta & \sin\beta \cos\theta \\ \sin\alpha \sin\beta & -\cos\alpha \sin\beta & \cos\beta \end{pmatrix}.
$$

In the case where the crystal orientation rotates around the x_3 axis, the transformation matrix R can be expressed as

$$
R = \begin{pmatrix} \cos\theta & \sin\theta & 0 \\ -\sin\theta & \cos\theta & 0 \\ 0 & 0 & 1 \end{pmatrix}. \tag{3}
$$

The relations between polarization components in local and global coordinate systems are expressed as

$$
p_i^L = R_{ij}p_j, \tag{4}
$$

where R_{ij} denotes the ij component of the transformation matrix R. The gradient energy density is given by

$$
f_{\mathrm{Grad}}(\nabla\boldsymbol{p}) = \frac{1}{2}\frac{\partial p_i}{\partial x_j}G_{ijkl}\frac{\partial p_k}{\partial x_l}, \tag{5}
$$

where G_{ijkl} is gradient tensor. The mechanical energy density is expressed as

$$
f_{\mathrm{Elas}}(\boldsymbol{\varepsilon}, \boldsymbol{p}) = \frac{1}{2}\left(\varepsilon_{ij} - \varepsilon_{ij}^0\right)c_{ijkl}\left(\varepsilon_{kl} - \varepsilon_{kl}^0\right), \tag{6}
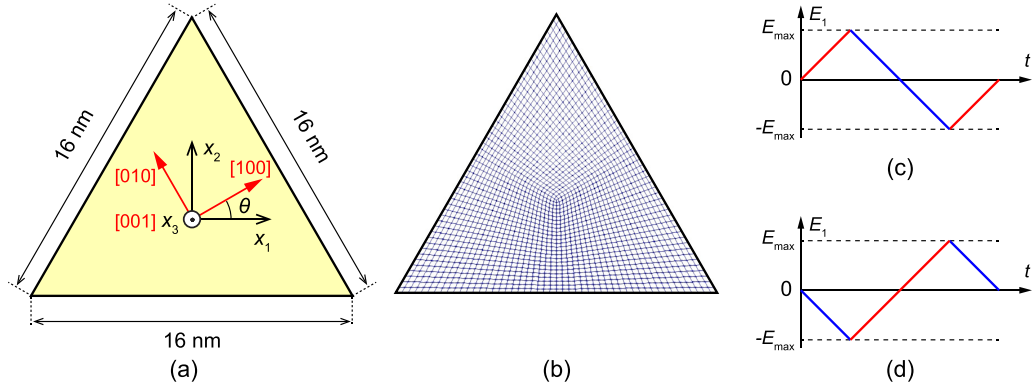$$

FIG. 1. (a) Schematic illustration of triangular ferroelectric nanodot and (b) its finite element meshing model. Triangular waves of electric field initiated with (c) positive and (d) negative electrical loading.

where c_{ijkl} is elasticity tensor. The spontaneous strain can be expressed with respect to the local coordinate system by $\varepsilon_{ij}^{0L} = Q_{ijkl} p_k^L p_l^L$, where Q_{ijkl} is electrostrictive coefficient. The spontaneous strain in global coordinate system can be obtained from

$$\varepsilon_{ij}^0 = R_{ik}^T \varepsilon_{kl}^{0L} R_{lj}. \tag{7}$$

The electrostatic energy density is expressed as

$$f_{\text{Elec}}(\boldsymbol{p}, \boldsymbol{\phi}) = -\frac{1}{2} \frac{\partial \phi}{\partial x_i} \varepsilon_0 \kappa_{ij} \frac{\partial \phi}{\partial x_j} + \frac{\partial \phi}{\partial x_i} p_i, \tag{8}$$

where ε_0 and κ_{ij} are the permittivity of vacuum and dielectric coefficient of background material, respectively.

The mechanical equilibrium equation for a body force-free ferroelectric is given by

$$\frac{\partial}{\partial x_j} \left(\frac{\partial f}{\partial \varepsilon_{ij}} \right) = 0. \tag{9}$$

The equilibrium of electric field for a charge-free ferroelectric is governed by the Maxwell's (or Gauss') equation, as

$$\frac{\partial}{\partial x_j} \left(-\frac{\partial f}{\partial E_i} \right) = 0, \tag{10}$$

where $E_i = -\partial \phi / \partial x_i$ is electric field. The evolution of polarization field is described by the time-dependent Ginzburg-Landau (TDGL) equation, as

$$\frac{\partial p_i(r, t)}{\partial t} = -\mathcal{L} \frac{\delta F}{\delta p_i(r, t)}, \tag{11}$$

where $\mathcal{L}$ is a kinetic coefficient; t and $r = (x_1, x_2, x_3)$ denote the evolution time and the spatial vector, respectively. Numerical algorithm based on the finite element method is used to solve the governing Eqs. (9), (10), and (11). The backward Euler scheme and Newton method are employed for time integration and nonlinear iteration scheme, respectively.

B. Simulation model and procedure

According to the geometry design approach, previous studies [23,24] suggested that the polarization vortex in a low-symmetric ferroelectric nanodot can be switched by a homogeneous electric field. In this study, a nanodot with triangular prism geometry is considered, namely triangular

nanodot. The cross-section of nanodot is an equilateral triangle, which exhibit the in-plane threefold symmetry. Such a triangular shape exhibits an incompatible characteristic with the in-plane fourfold symmetry of tetragonal ferroelectric phase, which may bring about a significant interaction between the crystal orientation and the outer shape of nanodot. To simulate the nanodot, a three-dimensional finite element model is constructed using hexahedral elements with average mesh size of 0.32 nm. The geometry and finite element model of the nanodot are illustrated in Fig. 1. To intentionally generate a vortex in the nanodot [1,38], the edge length of triangular nanodot is selected as 16 nm, while the thickness is 5 nm. Note that ferroelectric nanodots with dimensions down to 5 nm have been successfully fabricated thanks to the recent advances in manufacturing technology [39]. In addition, different geometries of ferroelectric nanodots have been experimentally achieved, including triangular prism [40], cube [39], dodecahedral shape [41], torus [42], and disk [43]. Therefore, the triangular nanodot with edge size of 16 nm is experimentally achievable. The origin of global coordinate system is located at the centroid of nanodot. The nanodot consists of a single crystal of tetragonal ferroelectric PbTiO$_3$, where the pseudocubic crystallographic [100] direction makes an angle θ to the x_1 axis and the [001] direction is coincident with the coordinate axis x_3. In this study, the crystal orientation is assumed to rotate about the x_3 axis; and the angle θ is considered in a range of [0, 360°]. The used material properties are adopted from previous studies [44]. In this study, we consider free-standing ferroelectric nanodots. To realize bare free surfaces of the nanodots, the electrical boundary conditions on all surfaces are set to be open-circuited, i.e., $Dn = 0$, so that the depolarizing fields from the polar surfaces are explicitly included. In addition, stress-free mechanical boundary conditions are imposed to the free surfaces of the nanodots. These electrical and mechanical boundary conditions have been widely used for free-standing ferroelectric nanostructures [21,22,25,26,45,46].

The initial state of polarization field is generated with a random distribution of infinitesimal polarization vectors. The evolution of polarization field toward its thermodynamic equilibrium at room temperature is determined by solving the TDGL equation. The stable domain structure is obtained when the change of total energy is as small as 10^{-3} eV, which is,
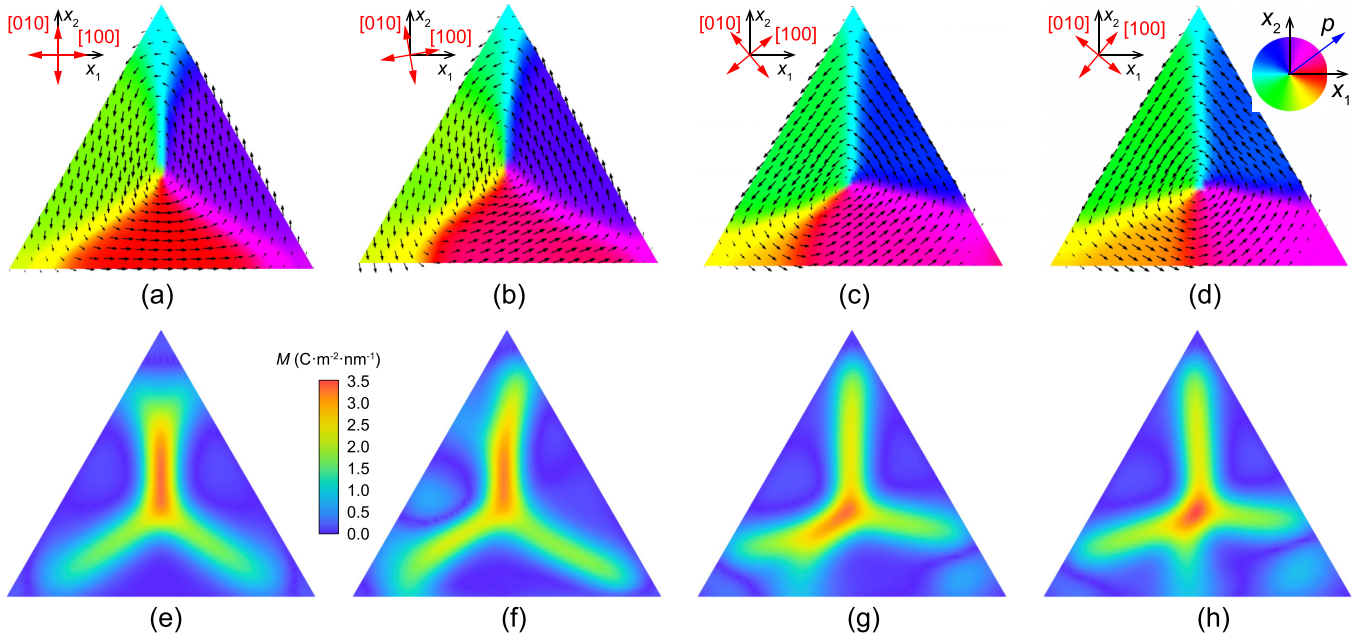
FIG. 2. Polarization vortex structures in triangular nanodots with different crystal orientations: (a) $\theta = 0°$, (b) $\theta = 10°$, (c) $\theta = 40°$, and (d) $\theta = 60°$. (e–h) Corresponding distributions of polarization vorticity.

otherwise, considered as a criterion for the thermodynamic equilibrium state. Then, an external homogeneous electric field E_1 is applied stepwise to the nanodot along the x_1 direction to consider the polarization switching. A triangular wave of electric field is used to consider the polarization switching. Depending on the switching behavior, the first loading process can proceed toward positive or negative electric field, as shown in Figs. 1(c) and 1(d), respectively. At each value of E_1, the simulation is carried out until the equilibrium domain structure is achieved.

III. RESULTS

A. Polarization vortex structures in triangular ferroelectric nanodots

Although the crystal orientation is considered in a full range of [0–360°], we present here four typical domain structures in the nanodots with $\theta = 0, 10, 40,$ and $60°$ [Figs. 2(a)–2(d)], according to their distinguishable switching behaviors that are detailed in the Sec. III B. The selected domain structures are sufficient to exhibit the effect of crystal orientation. In all considered nanodots, a single-vortex structure is spontaneously formed, where the polarization field continuously rotates around a core. In the absence of external field, the vortex core is located near the centroid of triangular nanodot, regardless of the crystal orientation. The polarization vectors arrange in the x_1x_2 plane, while the polarization component in the x_3 direction is suppressed due to the geometrical confinement [23]. In addition, such a ground state with vortex domain structure formed in the nanodot is attributed to the strong depolarization effect, similar to those emerged in ferroelectric nanodots with different geometries [1,10,23]. Since the cross-sections of domain structures in the x_3 direction are almost the same, we consistently present domain structures

in the x_1x_2 plane for clear illustrations. Experimental studies have demonstrated that the polarization vortex can be formed in ferroelectric nanodots [10,47]. Furthermore, in ferroelectric nanodots with plate geometry, polarization prefers to align in-plane, whereas the polarization component in the out-of-plane direction is suppressed [48,49]. Therefore, the formation of in-plane polarization vortex in the triangular nanodots is consistent. Although the single vortex forms in each considered nanodot, the local polarization vectors that are far from the vortex core mostly align along the ⟨100⟩ orientations, and thereby, exhibit a strong dependence on the crystal orientation. Although two equivalent vortex states, i.e., CCW and CW rotations, can appear in the nanodots, only CCW vortex state is shown in Figs. 2(a)–2(d) for a consistent illustration. To characterize the vorticity of polarization field, a toroidal moment along the x_3 direction is used and its magnitude is calculated as, $G_3 = V^{-1} \int_V r \times \boldsymbol{p}\, dV$. The overall toroidal moments are determined at 1.06, 1.11, 1.12, and 1.13 e/Å for the nanodots with $\theta = 0, 10, 40$ and $60°$, respectively. The calculated overall toroidal moments for the other crystal orientations achieve similar magnitudes. Thus, the overall toroidal moment of triangular nanodots is almost intact by the change of crystal orientation. To determine the position and direction of polarization vortex, distributions of vorticity (or curl) of polarization ($M = \nabla \times p$) are represented in Figs. 2(e)–2(h) for the representative nanodots. When $\theta = 0°$, the vorticity of polarization field highly concentrates at the vortex core. This result is reasonable since the polarization field near the vortex core deviates significantly from the spatial uniformity. In addition, the vorticity is large in areas from the vortex core toward three corners of triangular nanodots. The shape of areas with large vorticity alters according to the crystal orientation. Therefore, the change of crystal orientation slightly alters the overall characteristics of polarization
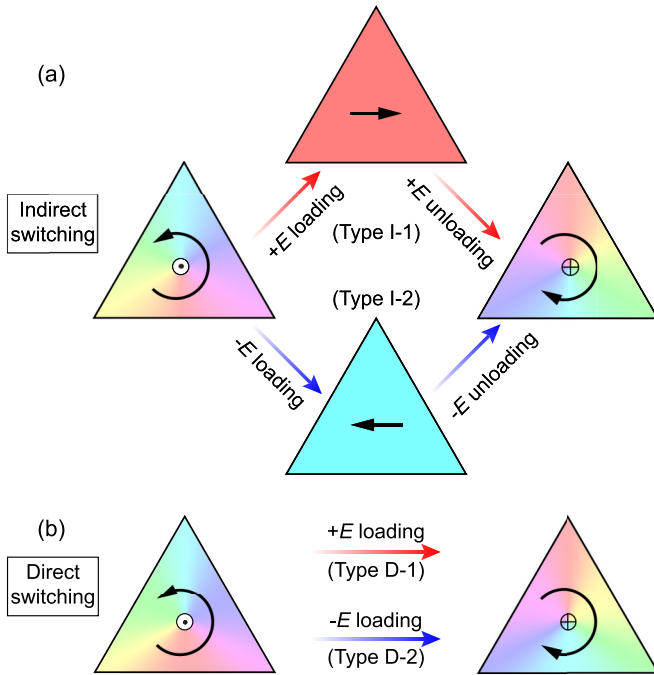
FIG. 3. Schematic illustration of possible pathways for the vortex switching under homogeneous electric field E_1: (a) indirect and (b) direct switching pathways.

vortex, but significantly affects the local ones. In the following subsections, we demonstrate that such a local effect gives rise to distinguishable switching behaviors of polarization vortex.

B. Vortex switching in triangular nanodots under homogeneous electric field

Given the single vortex formed in the nanodots, the vortex switching is investigated by applying a triangular wave of homogeneous electric field E_1 along the x_1 direction. Before we detail the vortex switching behaviors in the triangular nanodots with different crystal orientations, a schematic that illustrates some possible pathways for the vortex switching is represented in Fig. 3 for clarity purpose. The switching pathways can be separated into two classes; these are indirect and direct switching pathways. In the former class [Fig. 3(a)], the vortex rotation can be switched from one to another state through an intermediate nonvortex state. For example, the initial CCW vortex state is cleared away by forming a rectilinear domain during the electrical loading process. Then, the rectilinear domain transforms to a CW vortex state during the unloading process. Such a switching pathway can be proceeded by the loading processes of positive or negative electric fields, which are named as types I-1 and I-2, respectively [Fig. 3(a)]. In the latter class [Fig. 3(b)], the vortex rotation can be directly switched back and forth between CCW and CW states. Two types of direct switching can be obtained with the use of positive or negative electric fields in the loading process, named as types D-1 and D-2, respectively. Since the indirect pathway has been reported in most previous

studies, the switching behavior of vortex in triangular nanodot that follows this pathway is first presented.

1. Indirect switching of polarization vortex: Type I-1

Here, the indirect switching of polarization vortex that follows the type I-1 is presented. In Fig. 4(a), the toroidal moment G_3 is represented as a function of applied electric field E_1 for the triangular nanodot with $\theta = 0°$. The initial state of polarization pattern is taken with the CCW vortex, which is relaxed to equilibrium, as shown in Fig. 2(a). The first loading process is started with positive electric field. For clarity, typical domain structures of nanodot during the first electrical loading and unloading processes are represented in Fig. 4(b), which are marked by several points from K0 to K4. At the initial state, the toroidal moment achieves a high value of 1.06 e/Å. In the loading process, as E_1 increases from 0 to 0.1 V/Å, the toroidal moment G_3 gradually decreases to 0.67 e/Å, then suddenly drops to a zero value at $E_1 = 0.054$ V/Å. The domain structure at point K1 indicates that the reduction of G_3 is accompanied by the decrease of vortex area since the polarization vectors near the bottom edge of nanodot align the electric field direction in a large area. At $E_1 = 0.054$ V/Å, the initial CCW vortex is cleared away due to the formation of a rectilinear domain (K2), in which all polarization vectors align along the direction of electric field. Here, the electric field required for the vortex transformation is regarded as coercive electric field, $E_C = 0.054$ V/Å. The formation of rectilinear domain leads to the zero value of toroidal moment as $E_1 \geqslant 0.054$ V/Å. In the unloading process, when E_1 decreases from 0.1 to 0 V/Å, the toroidal moment G_3 keeps a zero value as $E_1 \geqslant 0.044$ V/Å, then decreases to a negative value at a lower field. The corresponding domain structure (K3) indicates the transformation of rectilinear domain to a polarization vortex. A careful observation of polarization evolution exhibits that the polarization vectors near the bottom edge of triangle reverse their orientations at the beginning of evolution. This local change of polarization forms a small vortex structure near the bottom edge (K3). The reformation of vortex structure from the rectilinear domain is clarified in previous study [23]. When the applied electric field decreases, the newly formed vortex becomes larger and its core moves toward the centroid of nanodot. At the zero field, the newly formed vortex dominates the domain structure of the nanodot. Consequently, the toroidal moment gradually decreases to −1.06 e/Å in the unloading process. Importantly, the newly formed vortex has the CW rotation, which is inverse to the initial CCW state. Similarly, the vortex switching from CW to CCW states can be achieved through the loading and unloading of negative electric field, as shown in Fig. 4(a). Therefore, the switching process occurs successively with a transformation of initial CCW vortex to rectilinear domain in the positive loading process and a reformation of CW vortex from the rectilinear domain in the unloading process. The switching behavior of polarization vortex in the triangular nanodot with $\theta = 0°$ is similar to that occurs in the antinotched nanodot, which is reported in the previous study [23]. Note that, the formation of rectilinear domain at large field is prerequisite to the vortex switching in the triangular nanodot with $\theta = 0°$.
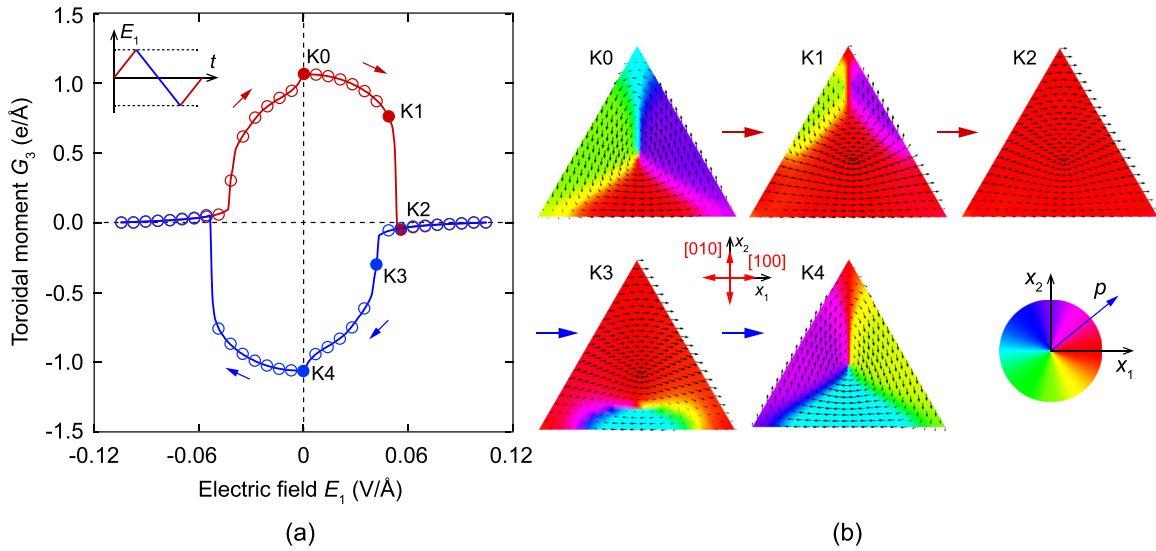
FIG. 4. Switching behavior of polarization vortex under homogeneous electric field in the triangular nanodot with $\theta = 0°$. (a) The toroidal moment G_3 as a function of electric field E_1. (b) Equilibrium domain structures at different magnitudes of electric field.

This switching behavior belongs to the switching type I-1, as schematically illustrated in Fig. 3(a).

2. Indirect switching of polarization vortex: Type I-2

In Fig. 5, the domain evolution of the nanodot with $\theta = 60°$ under homogeneous electric field E_1 is presented. Based on the preliminary simulations, to obtain a complete switching loop in one periodic of applied field, the first loading process should be initiated with the negative electric field. The initial polarization structure also adopts the CCW vortex state with the toroidal moment of 1.13 e/Å, as depicted in Fig. 2(d). At the first loading process from 0 to -0.1 V/Å, the toroidal moment decreases with decreasing electric field. In this process, the CCW vortex state first transforms into a wavy domain structure (L1). The formation of wavy domain structure orig-

inates from competitive effects of electric field and crystal orientation on polarization directions, in which the overall polarization direction tends to follow the electric field, while the local polarization vectors energetically prefer the $\langle 100 \rangle$ crystal orientations. At point L1, most polarization vectors arrange in the [$\bar{1}$00] and [010] crystal orientations. At $E_1 = -0.085$ V/Å, the wavy domain structure is switched to a rectilinear domain (L2), where the polarization vectors arrange along with the [010] crystal orientation. The stabilization of [010] single domain at large electric field is reasonable since the [010] orientation in the nanodot with $\theta = 60°$ is closer to the electric field direction (i.e., $-x_1$ direction) than that of the [$\bar{1}$00] orientation. The coercive electric field is determined as $E_C = -0.085$ V/Å. As a result, the toroidal moment drops to zero value. In the unloading process, as E_1 increases from -0.1 to 0 V/Å, the rectilinear domain remains until $E_1 =$
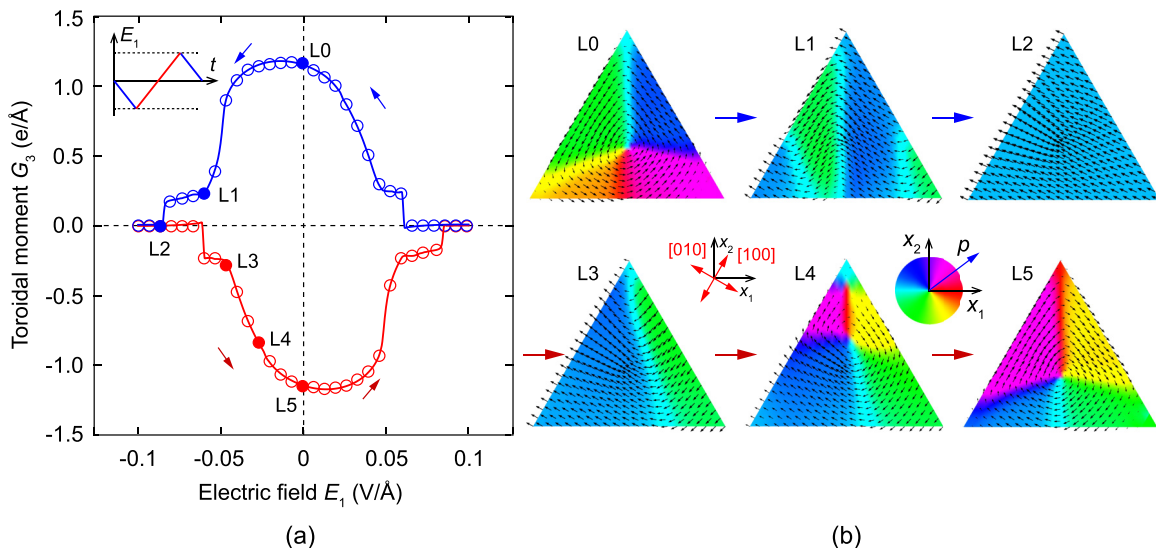

FIG. 5. Switching behavior of polarization vortex under homogeneous electric field in the triangular nanodot with $\theta = 60°$. (a) The toroidal moment G_3 as a function of electric field E_1. (b) Equilibrium domain structures at different magnitudes of electric field.

FIG. 6. Polarization vortex switching in the nanodot with $\theta = 40°$. (a) The toroidal moment G_3 as a function of electric field E_1. (b) Equilibrium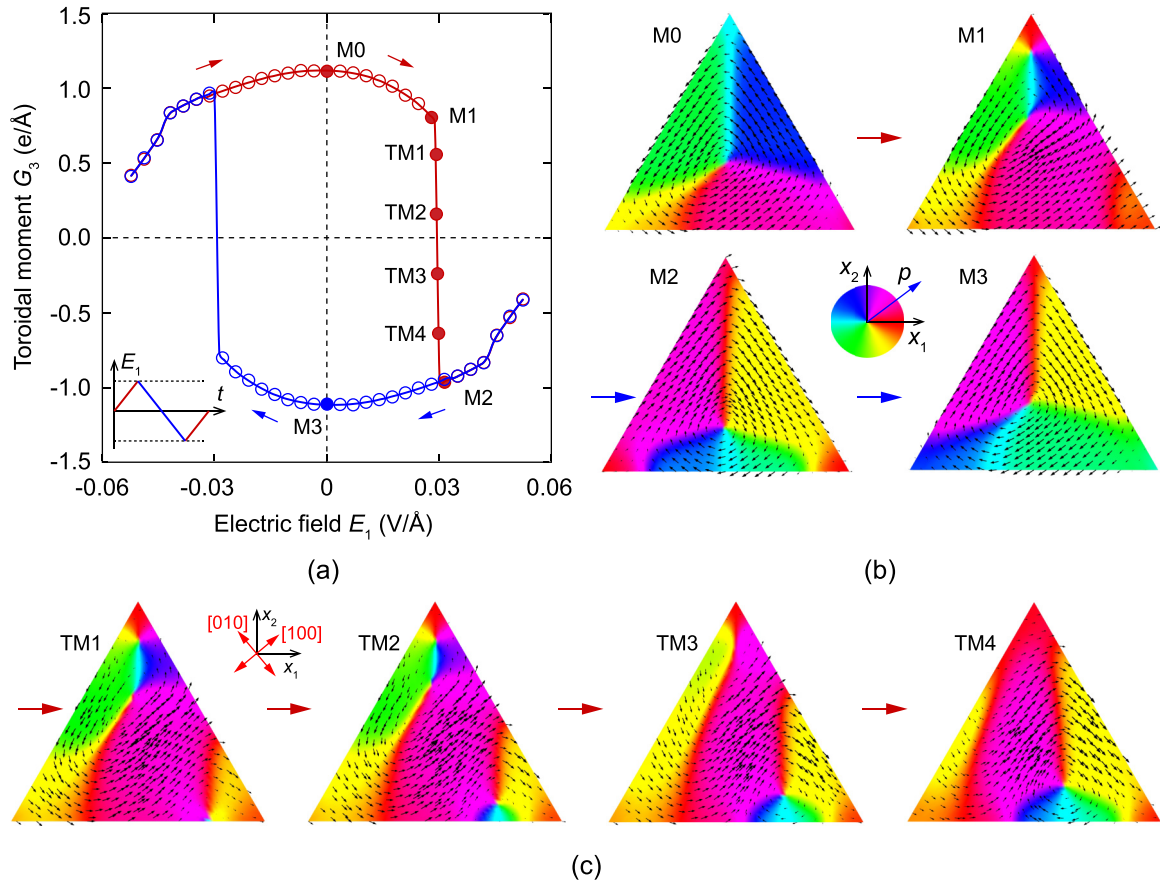 domain structures at different magnitude of electric field. (c) Snapshots of temporal domain structure during the vortex switching.

-0.06 V/Å, then transforms into a V-shaped domain structure (L3). Note that, such a V-shaped domain structure possesses a large polarization gradient, leading to a nonzero value of toroidal moment. At a lower field, the V-shaped domain structure transforms into a single vortex (L4). The newly formed vortex has CW rotation, which is opposite to the initial CCW state. It is obvious that the polarization vectors of the vortex structure at point L4 remains their orientations in a large area in comparison to that in the V-shaped domain structure, except for the top corner of triangular nanodot. Therefore, the formation of polarization vortex from the V-shaped domain structure becomes easy; and the rotation of newly formed vortex is determined by the V-shaped domain structure. A switching from CW to CCW vortex state occurs similarly under the positive electric loading and unloading processes. The vortex switching in the nanodot with $\theta = 60°$ exhibits a complex behavior, in which the vortex transformation passes through several intermediate nonvortex states, including wavy, rectilinear, and V-shaped domain structures. Note that, the stabilization of wavy and V-shaped domain structures at a moderate electric field originates from competitive effects of electric field and crystal orientation on polarization directions [50]. However, if the first loading process initiates with positive electric field on the CCW vortex, then the vortex orientation cannot be switched in the first half periodic of the applied electric field. However, the switching of CCW vortex

can be achieved after the first half periodic of the applied electric field. In this study, to avoid the potential confusion on the vortex switching, we choose the initial loading started with negative electric field, where a complete switching loop can be obtained in one periodic of applied field. The results shown in Fig. 5 demonstrate a deterministic switching of polarization vortex in the triangular nanodot with $\theta = 60°$. This switching behavior is regarded as the type I-2.

3. Direct switching of polarization vortex: Type D-1

In this subsection, the switching behavior of polarization vortex in the nanodot with $\theta = 40°$ under a homogeneous electric field is investigated. The loading process begins with an increase of positive electric field. The maximum of electric field is selected as 0.05 V/Å, which is large enough for the vortex switching. The initial state is taken with the CCW vortex. The switching behavior of polarization vortex is shown in Fig. 6. In the first increase of electric field from 0 to 0.05 V/Å, the toroidal moment G_3 gradually decreases from 1.12 to 0.77 e/Å, then suddenly drops to a large negative value of -0.86 e/Å at $E_1 = 0.03$ V/Å. The sudden change in the sign of toroidal moment is associated with the reversal of vortex rotation from CCW (M1) to CW (M2) states, which, otherwise, demonstrates the direct switching of polarization vortex. The newly formed CW vortex remains its rotation during the
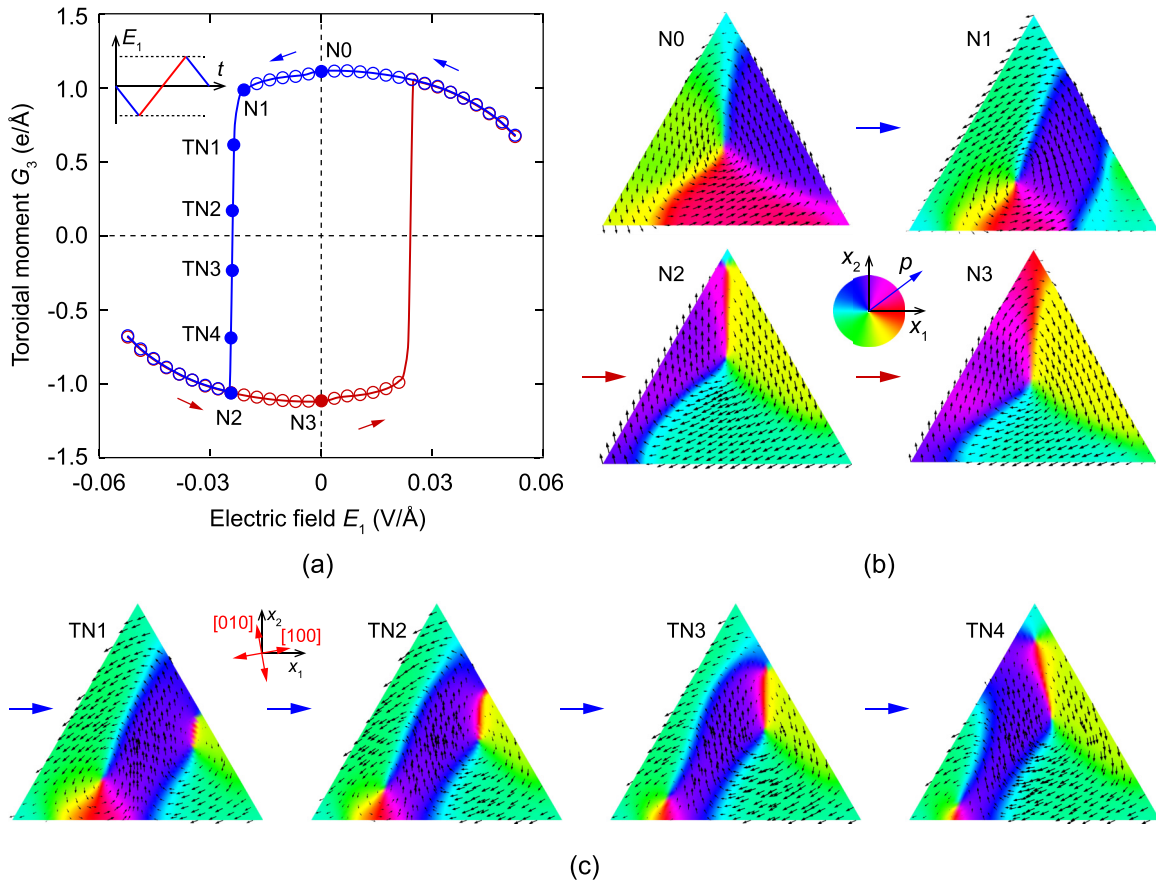
FIG. 7. Polarization vortex switching in the nanodot with $\theta = 10°$. (a) The toroidal moment G_3 as a function of electric field E_1. (b) Equilibrium domain structures at different magnitude of electric field. (c) Snapshots of temporal domain structure during the vortex switching.

unloading process (M3). Notably, the switching field $E_C = 0.03$ V/Å is much smaller than those in the switching types I-1 and I-2. In the indirect pathways, the switching process of vortex takes place through one or several intermediate states, in which the domain structure is distinguished from vortex structure, e.g., rectilinear, wavy, or V-shaped domain structures. In addition, the intermediate states are maintained in a wide range of electric field, and are prerequisite for the vortex switching to occur. However, the single vortex in the nanodot $\theta = 40°$ can be directly switched from CCW to CW rotations and vice versa without the stabilization of any intermediate state. This result exhibits a striking behavior of the switching in the nanodot with $\theta = 40°$ under homogeneous electric field and demonstrates the significant effect of crystal orientation on the vortex switching behavior. This switching behavior is regarded as type D-1.

To characterize and elucidate the detail on how the direct vortex switching takes place in the nanodot with $\theta = 40°$, temporal evolution of domain structure at $E_1 = 0.03$ V/Å in the loading process is considered. In Fig. 6(c), typical snapshots of domain structure during the polarization evolution are represented and marked by several points from TM1 to TM4. At the early evolution, the polarization vectors near the right corner of nanodot depart from the [100] domain and form a local curl polarization field (TM1). Then, a small polarization vortex with CW rotation is formed near the right corner of

nanodot, which coexists with the original CCW vortex (TM2). The CW vortex gradually expands, while the CCW vortex shrinks (TM3). At point TM4, the CW vortex dominates the domain structure of nanodot, while the original CCW vortex disappears. At the end of evolution, only CW vortex remains, and the switching of vortex rotation is obtained. It is obvious in Fig. 6(c), the domain structure also tends to form a wavy configuration under the electric field due to competitive effects of electric field and crystal orientation, similar to that in the nanodot with $\theta = 60°$. However, the truncation of wavy domain configuration due to the free edges of the nanodot with $\theta = 40°$ creates a local distinguishable region in the polarization field near the right corner of nanodot that facilitates the formation of local vortex structure. Therefore, the vortex switching behavior in the nanodot with $\theta = 40°$ is distinguished from that with $\theta = 60°$, although the crystal orientation in these two cases closes to each other.

4. Direct switching of polarization vortex: Type D-2

In Fig. 7, the switching behavior of polarization vortex in the nanodot with $\theta = 10°$ under a homogeneous electric field is presented. Based on the preliminary simulations, the electric field should be started with a negative electrical loading; and the maximum of applied electric field is selected as 0.05 V/Å. The initial state polarization pattern is taken with
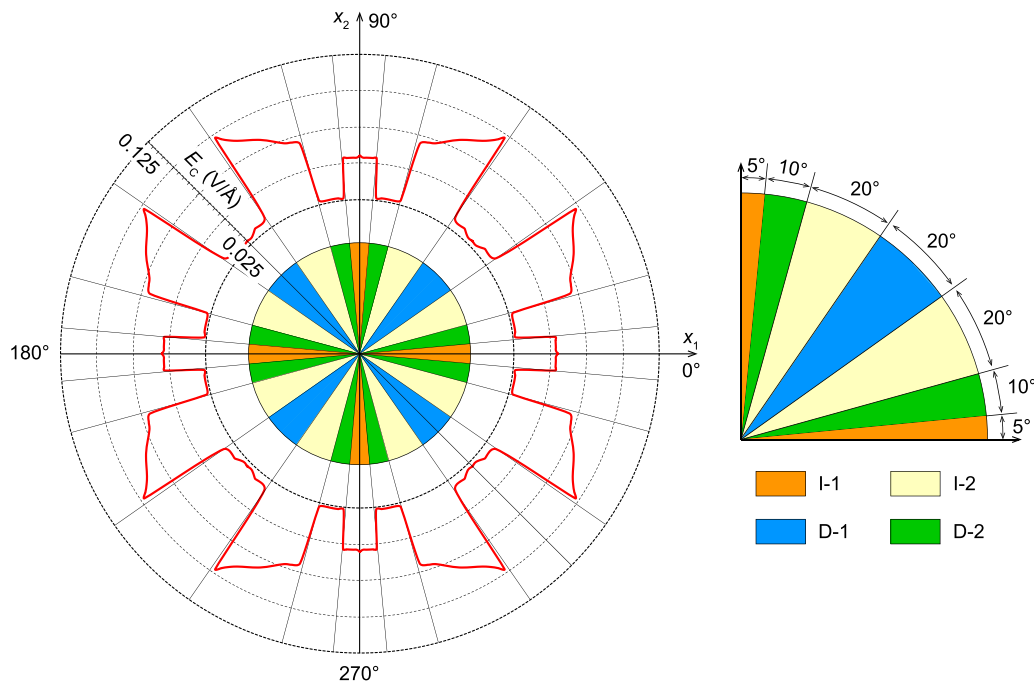
FIG. 8. Dependence of switching behavior and electric coercive field E_C on the crystal orientation (θ) in the triangular nanodot.

the CCW rotation (N0). In the first decrease process of negative electric field, the toroidal moment G_3 gradually decreases from 1.11 to 0.76 e/Å, then suddenly drops to a negative value of -1.05 e/Å at $E_1 = -0.025$ V/Å. The sudden change in the sign of toroidal moment originates from the CCW-to-CW vortex switching, as illustrated at points N1 and N2. This result clearly indicates the direct switching of vortex. The electric field required for the vortex switching E_c is relatively small in comparison to those in the indirect pathways. The rotation of CW vortex state remains when the electric field reduces to zero value (N3). The vortex structure in the triangular nanodot $\theta = 10°$ is also switched directly from CCW to CW rotations and vice versa without the stabilization of any intermediate state. Although the vortex switching behavior in nanodot with $\theta = 10°$ is similar to that in nanodot with $\theta = 40°$, the direction of electric field that triggers the vortex switching is opposite. This switching behavior follows the switching type D-2.

To clarify the direct switching behavior in the nanodot with $\theta = 10°$, temporal evolution of domain structure at the switching field $E_1 = -0.025$ V/Å in the loading process is considered. Typical snapshots of domain structure during the polarization evolution, which are marked by several points from TN1 to TN4, are represented in Fig. 7(c). As shown in Fig. 7(c) at point TN1, the polarization vectors near the lower junction between the domain wall and the right free edge change their directions at the beginning of evolution. Such a change of polarization vectors initiates the formation of a CW vortex near the junction (TN1). The CW vortex gradually expands, while the original CCW vortex shrinks (TN2 and TN3). At point TN4, the CW vortex dominates the domain structure of nanodot, while the original CCW vortex fades away. At the end of evolution, only CW vortex remains, and the switching of vortex rotation is obtained (N2).

C. Effect of crystallographic orientation on the vortex switching

To provide a more general perspective on the effect of crystal orientation on the vortex switching, here we summarize the angular dependence of switching pathways in the range of θ from 0 to 360°, as shown in Fig. 8. The background color in Fig. 8 indicates the angular span where a specific switching pathway can take place. As shown in Fig. 8, the polarization vortex in triangular nanodot can be switched directly or indirectly in the full range of θ. This result demonstrates that the triangular geometry of nanodot can guarantee the deterministic switching of polarization vortex under a homogeneous electric field. However, the switching behavior follows different pathways, depending on the magnitude of θ. More specifically, in the range of $[0,90°]$, the vortex switching follows the type I-1 in $[0,5°]$ and $[85,90°]$, type I-2 in $[15,35°]$ and $[55,75°]$, type D-1 in $[35,55°]$, and type D-2 in the remained ranges, as shown in the enlarged view in Fig. 8. In the full range of $[0,360°]$, the dependence of switching behavior on the crystal orientation exhibits fourfold symmetry. Hence, the results shown in Fig. 8 provides a helpful guideline for tailoring and achieving various switching behaviors of polarization vortex in the triangular nanodots.

Furthermore, we also present in Fig. 8 the angular dependence of switching field E_C, which is illustrated by a continuous curved line. The magnitude of switching field strongly depends on the crystal orientation. The E_C magnitude varies in a wide range from 0.025 to 0.1 V/Å. Importantly, the E_C magnitude in the direct types of vortex switching is much smaller than that of indirect ones. For example, the E_C magnitudes in the switching types D-1 and D-2 are about 0.025 V/Å, while those in the switching types I-1 and I-2 are larger than 0.05 V/Å. This result is reasonable since the direct switching pathways can take place without the destruction of vortex structure, which commonly requires a large electric

field due to the topological-protection property. In addition, this result suggests an effective pathway to switch the polarization vortex, which requires low-energy consumption. However, the desired ferrotoroidic properties for memory applications simultaneously require a high remanent toroidal moment and a low switching field. Since the direct switching pathways can proceed at a small coercive field while preserving the high magnitude of the remanent toroidal moment, one can improve the ferrotoroidic properties for memory applications by using rational crystal orientation in the triangular nanodots.

Recently, the polarization vortices in $PbTiO_3/SrTiO_3$ superlattice films are experimentally demonstrated to mobile and can be switched to ordinary single ferroelectric domains under an applied electric field [31]. After removal of the external field, the vortex structure spontaneously recovers [31]. These experimental results demonstrate the indirect switching of polarization vortex under electric field. However, in magnetic materials, the switching of magnetization vortex is experimentally observed in a triangular nanodot under in-plane magnetic field [51,52]. In ferroelectrics, as an analog material class of magnetics, the switching of polarization vortex in the triangular nanodot under in-plane electric field can occur similarly. Therefore, the switching pathways described in this study are reasonable.

However, several extrinsic effects may influence the vortex switching in ferroelectric nanodots. For example, the surface effect is one of important factors affecting the polarization behavior in ferroelectric nanodots since the charge screening tends to decrease the depolarization field inside the nanodots. In addition, ferroelectric nanodots are commonly fabricated on substrates, which gives rise to epitaxial strain. Since strain interacts with both polarization and toroidal moment through the electromechanical coupling [53], the substrate-induced strain may alter the polarization vortex switching under homogeneous electric field. However, a quantitative consideration for the influences of electrical and mechanical boundary conditions on the switching behavior of polarization vortex in triangular nanodots is kept for future work. Furthermore, the

size effect that also influences the stability of polarization vortex and the vortex switching should be considered. For example, our preliminary simulations suggest that the polarization vortex is stably formed in triangular nanodots with the edge size below 40 nm. Although the results presented in Fig. 8 specific for triangular nanodot, a similar results can be obtained for diversity of nanodot geometries with odd-fold symmetries. Therefore, this study opens exciting opportunities for optimizing the vortex switching behavior with low-power consumption and short switching duration through a rational control of crystal orientation incompatible to geometries of ferroelectric nanostructures.

IV. CONCLUSION

In summary, we performed a systematic investigation on the dynamics of polar vortex in triangular $PbTiO_3$ nanodots with different crystal orientations under a homogeneous electric stimulus, using phase field model based on Ginzburg-Landau theory. The polarization vortex and its characteristics are considered in a wide range of crystal orientation. The obtained results demonstrate that the vortex rotation in a triangular nanodot can be switched by a homogeneous electric field, regardless of the crystal orientation. However, the change of crystal orientation significantly tailors the switching behaviors, in which the vortex rotation can be switched directly or indirectly. The indirect switching pathway requires the stabilization of intermediate states, while the direct one takes place without them. In addition, the direct switching pathway requires lower electric field in comparison to that of indirect one, suggesting an effective route to switch the polarization vortex. Furthermore, this study demonstrates that the incompatibility between the crystal orientation and geometry of ferroelectric nanostructures provides a new degree of freedom to engineer the dynamic behavior of polarization vortex under external fields, which, otherwise, is potentially adopted to control the dynamic behavior of different topological defects.

[1] I. I. Naumov, L. Bellaiche, and H. Fu, Unusual phase transitions in ferroelectric nanodisks and nanorods, Nature (London) **432**, 737 (2004).

[2] S. Das, Y. L. Tang, Z. Hong, M. A. P. Gonçalves, M. R. McCarter, C. Klewe, K. X. Nguyen, F. Gómez-Ortiz, P. Shafer, E. Arenholz *et al.*, Observation of room-temperature polar skyrmions, Nature (London) **568**, 368 (2019).

[3] L. Li, X. Cheng, J. R. Jokisaari, P. Gao, J. Britson, C. Adamo, C. Heikes, D. G. Schlom, L.-Q. Chen, and X. Pan, Defect-Induced Hedgehog Polarization States in Multiferroics, Phys. Rev. Lett. **120**, 137602 (2018).

[4] Y. J. Wang, Y. P. Feng, Y. L. Zhu, Y. L. Tang, L. X. Yang, M. J. Zou, W. R. Geng, M. J. Han, X. W. Guo, B. Wu *et al.*, Polar meron lattice in strained oxide ferroelectrics, Nat. Mater. **19**, 881 (2020).

[5] J. Seidel, Nanoelectronics based on topological structures, Nat. Mater **18**, 188 (2019).

[6] G. F. Nataf, M. Guennou, J. M. Gregg, D. Meier, J. Hlinka, E. K. H. Salje, and J. Kreisel, Domain-wall engineering and topological defects in ferroelectric and ferroelastic materials, Nat. Rev. Phys. **2**, 634 (2020).

[7] S. Chen, S. Yuan, Z. Hou, Y. Tang, J. Zhang, T. Wang, K. Li, W. Zhao, X. Liu, L. Chen *et al.*, Recent progress on topological structures in ferroic thin films and heterostructures, Adv. Mater. **33**, 2000857 (2020).

[8] C.-L. Jia, K. W. Urban, M. Alexe, D. Hesse, and I. Vrejoiu, Direct observation of continuous electric dipole rotation in flux-closure domains in ferroelectric Pb(Zr,Ti)O₃, Science **331**, 1420 (2011).

[9] A. K. Yadav, C. T. Nelson, S. L. Hsu, Z. Hong, J. D. Clarkson, C. M. Schlepütz, A. R. Damodaran, P. Shafer, E. Arenholz, L. R. Dedon *et al.*, Observation of polar vortices in oxide superlattices, Nature (London) **530**, 198 (2016).

[10] D. Karpov, Z. Liu, T. dos Santos Rolo, R. Harder, P. V. Balachandran, D. Xue, T. Lookman, and E. Fohtung, Three-dimensional imaging of vortex structure in a ferroelectric nanoparticle driven by an electric field, Nat. Commun. **8**, 280 (2017).

[11] N. D. Mermin, The topological theory of defects in ordered media, Rev. Mod. Phys. **51**, 591 (1979).

[12] L. Van Lich, T. Q. Bui, T. Shimada, T. Kitamura, T.-G. Nguyen, and V.-H. Dinh, Deterministic switching of polarization vortices in compositionally graded ferroelectrics using a mechanical field, Phys. Rev. Appl. **11**, 054001 (2019).

[13] N. Balke, B. Winchester, W. Ren, Y. H. Chu, A. N. Morozovska, E. A. Eliseev, M. Huijben, R. K. Vasudevan, P. Maksymovych, J. Britson et al., Enhanced electric conductivity at ferroelectric vortex cores in $BiFeO_3$, Nat. Phys. **8**, 81 (2012).

[14] W. Yang, G. Tian, Y. Zhang, F. Xue, D. Zheng, L. Zhang, Y. Wang, C. Chen, Z. Fan, Z. Hou et al., Quasi-one-dimensional metallic conduction channels in exotic ferroelectric topological defects, Nat. Commun. **12**, 1306 (2021).

[15] S. Prosandeev, A. Malashevich, Z. Gui, L. Louis, R. Walter, I. Souza, and L. Bellaiche, Natural optical activity and its control by electric field in electrotoroidic systems, Phys. Rev. B **87**, 195111 (2013).

[16] F. Zhuo and C.-H. Yang, Observation of a stable fractionalized polar skyrmionlike texture with giant piezoelectric response enhancement, Phys. Rev. B **102**, 214112 (2020).

[17] A. K. Yadav, K. X. Nguyen, Z. Hong, P. García-Fernández, P. Aguado-Puente, C. T. Nelson, S. Das, B. Prasad, D. Kwon, S. Cheema et al., Spatially resolved steady-state negative capacitance, Nature (London) **565**, 468 (2019).

[18] S. Das, Z. Hong, V. A. Stoica, M. A. P. Gonçalves, Y.-T. Shao, E. Parsonnet, E. J. Marksz, S. Saremi, M. R. McCarter, A. Reynoso et al., Local negative permittivity and topological phase transition in polar skyrmions, Nat. Mater. **20**, 194 (2021).

[19] V. M. Dubovik and V. V. Tugushev, Toroid moments in electrodynamics and solid-state physics, Phys. Rep. **187**, 145 (1990).

[20] I. I. Naumov and H. Fu, Cooperative Response of Pb(ZrTi)O₃ Nanoparticles to Curled Electric Fields, Phys. Rev. Lett. **101**, 197601 (2008).

[21] S. Prosandeev, I. Ponomareva, I. Kornev, I. Naumov, and L. Bellaiche, Controlling Toroidal Moment by Means of an Inhomogeneous Static Field: An ab initio Study, Phys. Rev. Lett. **96**, 237601 (2006).

[22] J. Liu, Y. Ji, S. Yuan, L. Ding, W. Chen, and Y. Zheng, Controlling polar-toroidal multi-order states in twisted ferroelectric nanowires, NPJ Comput. Mater. **4**, 78 (2018).

[23] L. Van Lich, T. Shimada, J. Wang, V.-H. Dinh, T. Q. Bui, and T. Kitamura, Switching the chirality of a ferroelectric vortex in designed nanostructures by a homogeneous electric field, Phys. Rev. B **96**, 134119 (2017).

[24] H. Dinh-Van, L. V. Lich, T. Q. Bui, T. Van Le, T.-G. Nguyen, T. Shimada, and T. Kitamura, Intrinsic and extrinsic effects on the electrotoroidic switching in a ferroelectric notched nanodot by a homogeneous electric field, Phys. Chem. Chem. Phys. **21**, 25011 (2019).

[25] W. J. Chen and Y. Zheng, Vortex switching in ferroelectric nanodots and its feasibility by a homogeneous electric field: Effects of substrate, dislocations and local clamping force, Acta Mater. **88**, 41 (2015).

[26] S. Yuan, W. J. Chen, L. L. Ma, Y. Ji, W. M. Xiong, J. Y. Liu, Y. L. Liu, B. Wang, and Y. Zheng, Defect-mediated vortex multiplication and annihilation in ferroelectrics and the feasibility of vortex switching by stress, Acta Mater. **148**, 330 (2018).

[27] L. V. Lich, M.-T. Le, T. Q. Bui, T.-T. Nguyen, T. Shimada, T. Kitamura, T.-G. Nguyen, and V.-H. Dinh, Asymmetric flux-closure domains in compositionally graded nanoscale ferroelectrics and unusual switching of toroidal ordering by an irrotational electric field, Acta Mater. **179**, 215 (2019).

[28] A. R. Damodaran, J. D. Clarkson, Z. Hong, H. Liu, A. K. Yadav, C. T. Nelson, S.-L. Hsu, M. R. McCarter, K.-D. Park, V. Kravtsov et al., Phase coexistence and electric-field control of toroidal order in oxide superlattices, Nat. Mater. **16**, 1003 (2017).

[29] K. Du, M. Zhang, C. Dai, Z. Zhou, Y. Xie, Z. Ren, H. Tian, L. Chen, G. Van Tendeloo, and Z. Zhang, Manipulating topological transformations of polar structures through real-time observation of the dynamic polarization evolution, Nat. Commun. **10**, 4864 (2019).

[30] P. Chen, X. Zhong, J. A. Zorn, M. Li, Y. Sun, A. Y. Abid, C. Ren, Y. Li, X. Li, X. Ma et al., Atomic imaging of mechanically induced topological transition of ferroelectric vortices, Nat. Commun. **11**, 1840 (2020).

[31] X. Li, C. Tan, C. Liu, P. Gao, Y. Sun, P. Chen, M. Li, L. Liao, R. Zhu, J. Wang et al., Atomic-scale observations of electrical and mechanical manipulation of topological polar flux closure, Proc. Natl. Acad. Sci. USA **117**, 18954 (2020).

[32] L. V. Lich, Q.-T. Ton, T.-G. Nguyen, and V.-H. Dinh, On the correlation between topological defects of polarization field and euler characteristics of ferroelectric nanostructures, Appl. Phys. Lett. **114**, 022901 (2019).

[33] L. L. Ma, Y. Ji, W. J. Chen, J. Y. Liu, Y. L. Liu, B. Wang, and Y. Zheng, Direct electrical switching of ferroelectric vortices by a sweeping biased tip, Acta Mater. **158**, 23 (2018).

[34] R. Xu, J. Karthik, A. R. Damodaran, and L. W. Martin, Stationary domain wall contribution to enhanced ferroelectric susceptibility, Nat. Commun. **5**, 3120 (2014).

[35] R. Xu, R. Gao, S. E. Reyes-Lillo, S. Saremi, Y. Dong, H. Lu, Z. Chen, X. Lu, Y. Qi, S.-L. Hsu et al., Reducing coercive-field scaling in ferroelectric thin films via orientation control, ACS Nano **12**, 4736 (2018).

[36] L.-Q. Chen, Phase-field method of phase transitions/domain structures in ferroelectric thin films: a review, J. Am. Ceram. Soc. **91**, 1835 (2008).

[37] S. Choudhury, Y. L. Li, C. E. Krill Iii, and L. Q. Chen, Phase-field simulation of polarization switching and domain evolution in ferroelectric polycrystals, Acta Mater. **53**, 5313 (2005).

[38] A. R. Balakrishna and J. E. Huber, Scale effects and the formation of polarization vortices in tetragonal ferroelectrics, Appl. Phys. Lett. **106**, 092906 (2015).

[39] M. J. Polking, M.-G. Han, A. Yourdkhani, V. Petkov, C. F. Kisielowski, V. V. Volkov, Y. Zhu, G. Caruntu, A. P. Alivisatos, and R. Ramesh, Ferroelectric order in individual nanometre-scale crystals, Nature Mater. **11**, 700 (2012).

[40] H. Nonomura, H. Fujisawa, M. Shimizu, H. Niu, and K. Honda, Self-assembled PbTiO₃ nano-islands prepared on SrTiO₃ by metalorganic chemical vapor deposition, Jpn. J. Appl. Phys. **42**, 5918 (2003).

[41] H. Zhan, X. Yang, C. Wang, J. Chen, Y. Wen, C. Liang, H. F. Greer, M. Wu, and W. Zhou, Multiple nucleation and crystal growth of barium titanate, Cryst. Growth Des. **12**, 1247 (2012).

[42] F. Xia, J. Liu, D. Gu, P. Zhao, J. Zhang, and R. Che, Microwave absorption enhancement and electron microscopy characterization of $BaTiO_3$ nano-torus, Nanoscale **3**, 3860 (2011).

[43] Z. Li, Y. Wang, G. Tian, P. Li, L. Zhao, F. Zhang, J. Yao, H. Fan, X. Song, D. Chen *et al.*, High-density array of ferroelectric nanodots with robust and reversibly switchable topological domain states, Sci. Adv. **3**, e1700919 (2017).

[44] M. J. Haun, E. Furman, S. J. Jang, H. A. McKinstry, and L. E. Cross, Thermodynamic theory of $PbTiO_3$, J. Appl. Phys. **62**, 3331 (1987).

[45] I. Naumov and A. M. Bratkovsky, Unusual polarization patterns in flat epitaxial ferroelectric nanoparticles, Phys. Rev. Lett. **101**, 107601 (2008).

[46] S. Prosandeev, A. R. Akbarzadeh, and L. Bellaiche, Discovery of incipient ferrotoroidics from atomistic simulations, Phys. Rev. Lett. **102**, 257601 (2009).

[47] B. J. Rodriguez, X. S. Gao, L. F. Liu, W. Lee, I. I. Naumov, A. M. Bratkovsky, D. Hesse, and M. Alexe, Vortex polarization states in nanoscale ferroelectric arrays, Nano Lett. **9**, 1127 (2009).

[48] L. J. McGilly and J. M. Gregg, Polarization closure in $PbZr_{(0.42)}Ti_{(0.58)}O_3$ nanodots, Nano Lett. **11**, 4490 (2011).

[49] A. Schilling, S. Prosandeev, R. G. P. McQuaid, L. Bellaiche, J. F. Scott, and J. M. Gregg, Shape-induced phase transition of domain patterns in ferroelectric platelets, Phys. Rev. B **84**, 064110 (2011).

[50] J. Wang, W. Shu, T. Shimada, T. Kitamura, and T.-Y. Zhang, Role of grain orientation distribution in the ferroelectric and ferroelastic domain switching of ferroelectric polycrystals, Acta Mater. **61**, 6037 (2013).

[51] M. Jaafar, R. Yanes, D. Perez de Lara, O. Chubykalo-Fesenko, A. Asenjo, E. M. Gonzalez, J. V. Anguita, M. Vazquez, and J. L. Vicent, Control of the chirality and polarity of magnetic vortices in triangular nanodots, Phys. Rev. B **81**, 054439 (2010).

[52] A. Vogel, A. Corinna Niemann, C. Stenner, A. Drews, M.-Y. Im, P. Fischer, and G. Meier, Vortex dynamics in triangular-shaped confining potentials, J. Appl. Phys. **112**, 063916 (2012).

[53] L. V. Lich, T. Shimada, S. Sepideh, J. Wang, and T. Kitamura, Polar and toroidal electromechanical properties designed by ferroelectric nano-metamaterials, Acta Mater. **113**, 81 (2016).